



Polypyrrole linear actuation tuned by phosphotungstic acid



Zane Zondaka^a, Arko Kesküla^a, Tarmo Tamm^a, Rudolf Kiefer^{b,*}

^a Institute of Technology, University of Tartu, Nooruse 1, 50411 Tartu, Estonia

^b Faculty of Applied Sciences, Ton Duc Thang University, Ho Chi Minh City, Viet Nam

ARTICLE INFO

Article history:

Received 21 October 2016

Received in revised form 9 March 2017

Accepted 13 March 2017

Available online 16 March 2017

Keywords:

PPy/DBS-PT

Linear actuators

Strain and stress

FTIR

Raman

ABSTRACT

Co-doping polypyrrole (PPy) with dodecylbenzenesulfonate and multicharged phosphotungstate anions (PT) from the phosphotungstic acid (PTA) led to free-standing PPy/DBS-PT films, which were studied for their linear actuation properties. FTIR and Raman spectra revealed that PT was successfully embedded in PPy/DBS during electropolymerisation. Isometric stress and isotonic strain measurements in aqueous electrolyte under various electrochemical experiments showed an increase in the obtainable strain and stress, which was attributed to the electrocatalytic role PTA plays during the electropolymerisation. This results in lower synthesis potential and the formation of more compact films in comparison to PPy/DBS films under equal conditions. With the improved structure as well as the higher-charged immobilized PT dopant, 17 times higher conductivities, 1.7 times higher redox charge, and 1.8 times higher specific capacitance were obtained (at equal frequency). Energy dispersive X-ray (EDX) spectra indicated that contrary to some other published works, the majority of PT stayed stably in the film during consecutive redox cycles.

© 2017 Elsevier B.V. All rights reserved.

1. Introduction

Linear conducting polymer (CP) actuators have been widely studied during the last decades [1–3] with main focus on optimization towards maximum strain and stress. PPy/LiTFSI and PPy/TBACF₃SO₃ linear actuators have shown strains as high as 20% [1,4] and stress in range of 10–20 MPa [4]. The main reasons why such actuators are not appearing in any real application has been due to the low efficiency and poor reliability of such materials. It has been shown that minor changes in the electropolymerisation process [5], electrolyte [4,6] or solvent [7–9] can significantly change the properties of the actuators. Conducting polymers are faradaic actuators where the amount of exchanged charge is linearly related to the actuation properties [6]. Common linear actuators are based on PPy doped with dodecylbenzenesulfonate (PPy/DBS), showing mainly cation-driven actuation [10] with strain in range of 2% and maximal stress around 0.5 MPa [11]. It has been shown that for the case of PPy/DBS trilayers, the actuation direction can be changed by replacing the solvent [12]: from cation driven in water to anion-driven in organic solvent. The actuation properties of linear conducting polymer films are also known to depend strongly on the electrolyte solution, a typical cation-driven PPy/DBS film can

be turned into anion-driven by changing solvent and electrolytes [13].

The incorporation of redox active and multi-charged POM in conducting polymer is expected to lead to improved charging/discharging properties [14]. Different opinions have been given in the literature [15] about the attachment of POM and conducting polymers, which could either be covalent bonding such as monomer fixation on POM; or forming ionic complexes by applying POM as the electrolyte during electropolymerization [16]. Polyoxometalates contain a specific metal-oxide structure with a general formula [M_xO_y]_n[−] (M = V, Mo, W) [17]. In most cases the Keggin type POM [PW₁₂O₄₀]^{3−} (PT) is applied in combination with PPy [18], leading to films with improved charging/discharging. PPy/DBS, a typical cation-driven actuator is chosen here to show the effects of POM (in our case PTA) on a well-known system. The improvement of charging/discharging of PPy/DBS-PT is assigned to the improved structure, leading to higher conductivity, but also to the immobilised highly-charged PT^{3−} in comparison to PPy/DBS where just DBS[−] is immobilised.

Applications drawn from these hybrid materials include electrochemical capacitors [15,19], where heteropolyacids (protonated POMs) are applied, with reported specific capacitance for PEDOT/PT in range of 31 F/g [20] and PPy/12-molybdosilicic acid (PMA) in range of 34 F/g [21]. Improvement of PPy/PMA using nanoporous chemical polymerized composites gave specific capacitance in the range of 700 F/g [19].

* Corresponding author.

E-mail address: rudolf.kiefer@tdt.edu.vn (R. Kiefer).

Photoelectrochromic devices [15], sensors [22], corrosion protection [23], and electrocatalysts [24] are some of the other common applications for CP-POM hybrids. A large variety of hybrids with combinations of different POM types and CPs like PPy, PEDOT and PANi have been made, to study their combined properties for improved charge and energy storage [17]. In some cases, POM has been applied to embed nano-particles such as metals or carbon based materials [25] in conducting polymers to enhance conductivity and stability [26].

Recent research has revealed that PTA was able to embed carbon particles (carbide-derived carbon) during electropolymerization forming PPy/DBS-CDC hybrids, which had increased maximum strain due to changing of the films elastic modulus [27]. The formation of PPy linear actuators (free-standing films) containing PTA as electrolyte has not been reported until now, mostly due to the extreme brittleness of these films. Here we report PPy/DBS-PT linear actuators to demonstrate the benefits of PTA to the maximum strain and stress in comparison to PPy/DBS linear actuators in aqueous electrolyte. Isometric stress and isotonic strain measurements under different electrochemical schemes (cyclic voltammetry, chronoamperometry and chronopotentiometry) were applied to evaluate the differences in charge density, strain and stress, and specific capacitance. Material characterizations were made by FTIR, Raman, SEM and EDX.

2. Material and methods

2.1. Materials

Sodium dodecylbenzenesulfonate (NaDBS, 99%), ethylene glycol (EG, 99.8%), bis(trifluoromethane)sulfonimide lithium salt (LiTFSI, 99.95%), phosphotungstic acid hydrate (PTA, $\text{PW}_{12}\text{O}_{40}^{3-}$, reagent grade) were supplied by Sigma-Aldrich and used as supplied. Pyrrole (Py, $\geq 98\%$) from Sigma-Aldrich was distilled prior to use and stored at -20°C in the dark.

2.2. Polymerization of PPy/DBS and PPy/DBS-PT

PPy/DBS was polymerized galvanostatically at 0.1 mA cm^{-2} (40,000 s at -20°C) in a 2-electrode cell with stainless steel mesh counter electrode and stainless steel sheet working electrode (18 cm^2) in 0.1 M NaDBS, 0.1 M Pyrrole in EG/Milli-Q (1:1) mixture. PPy/DBS-PT was polymerized under the same conditions but with the addition of 0.01 M phosphotungstic acid. Both films were peeled off from the stainless steel sheet after the polymerization finished, washed with ethanol to remove excess monomer and washed with Milli-Q to remove the excess of NaDBS. The films were stored in 0.2 M NaDBS EG:Milli-Q solution. The thickness of PPy/DBS films was $19\ \mu\text{m}$ and for PPy/DBS-PT films $23\ \mu\text{m}$.

2.3. Isotonic stress and isometric strain measurements

PPy/DBS and PPy/DBS-PT films were cut into strips of 15 mm length and 1 mm width. The weight of PPy/DBS and PPy/DBS-PT films (after 48 h in LiTFSI-aq electrolyte) was $224 \pm 18\ \mu\text{g}$ and $295 \pm 23\ \mu\text{g}$, respectively. The films were connected to a force sensor (TRI202PAD, Panlab) with a fixed arm that served as a working electrode in the linear muscle analyzer set up [28]. Platinum sheet was used as counter electrode and Ag/AgCl (3 M KCl) as reference electrode in the measurement cell (0.2 M LiTFSI-aq electrolyte). The initial length of the films between the clamps was 1 mm. The force (isometric, constant length of 1 mm) and length changes (isotonic, force of 9.8 mN, calculated as stress for PPy/DBS 0.52 MPa and for PPy/DBS-PT: 0.43 MPa) under applied electrical signal were measured in real time with self-written software. Within a voltage range of 0.65 V to -0.6 V , the cyclic voltammetry

(scan rate 5 mV s^{-1}), the chronoamperometry and the chronopotentiometry at constant charge of 1 mC (frequencies 0.0025 Hz, 0.005 Hz, 0.01 Hz, 0.025 Hz, 0.05 Hz and 0.1 Hz) were performed. The stiffness before film charging (PPy/DBS: 0.2 MPa, PPy/DBS-PT: 0.18 MPa), after 20 redox cycles (PPy/DBS: 0.11 MPa; PPy/DBS-PT: 0.12 MPa) and after nearly 600 actuation measurements (PPy/DBS: 0.07 MPa, PPy/DBS-PT: 0.09 MPa) was determined. Each complete measurement set up (force and strain) needs 8 h measurements time and contains cyclic voltammetry at different scan rates, chronoamperometry and chronopotentiometry at different frequencies, including one long term measurement of 400 cycles at 0.1 Hz.

2.4. Characterization of the films

PPy/DBS and PPy/DBS-PT films were analysed by FTIR (Alpha, Bruker) in oxidized state after 600 actuation cycles. Raman spectra were recorded by using a Renishaw in Via micro-Raman spectrometer (spectral resolution 2 cm^{-1}) employing the 514 nm line of an argon-ion laser for excitation and a 50x objective for focusing of the laser beam and collecting the backscattered Raman signal (films in oxidized state after 600 actuation cycles). SEM (Helios NanoLab 600, FEI) and EDX analysis were performed of the unactuated films, films in reduced state (polarized 5 for min at -0.8 V) and films in oxidized state ($+0.8\text{ V}$, 5 min) to determine the ions on the surface of the film and in the cross-section (films broken under liquid nitrogen). The conductivity of the films was determined by four-point probe method with a surface resistivity meter (Guardian SRM). The conductivity was calculated from equation: $\sigma = 1/(R \cdot w)$, where σ is the electric conductivity, R is surface resistivity (Ω/sq) and w is material thickness (μm).

3. Results and discussion

3.1. Polymerization of PPy/DBS and PPy/DBS-PT

A typical PPy/DBS galvanostatic deposition takes place in the aqueous solution of NaDBS and pyrrole monomer [13]. Polyoxometalates such as $\text{PW}_{12}\text{O}_{40}^{3-}$ engage as electro catalyst in solution during the polymerisation process forming a small amount of chemically polymerized PPy if the concentration of PTA is too high. Several attempts of synthesis with PTA as the sole supporting electrolyte in the deposition solution failed resulting in no solid PPy/PT films. Polymerization with 0.1 M PTA in NaDBS solution, however, did lead to film formation due to the plasticiser properties of NaDBS but the films were brittle and the removal from stainless steel was not possible (material broke in pieces). Therefore, we applied PPy/DBS polymerization with less PTA (0.01 M) and a solid film on stainless steel was obtained. The polymerization curves of PPy/DBS and PPy/DBS-PT are shown in Fig. 1.

During galvanostatic polymerization, the applied voltage reached the value of 2.2 V in the 2-electrode system [27]. It is notable that the addition of PTA results in lower synthesis potential in the range of 1.4 V [17]. The addition of PTA and lowered polymerization potential was assumed to lead to two effects on the polymer: a) denser PPy/DBS-PT films with fewer defects (due to lower synthesis potential); b) immobilised PT anions in the film influencing the charging/discharging properties [18] of the films. The SEM images of the surface and cross sections of PPy/DBS and PPy/DBS-PT free-standing films after polymerization are shown in Fig. 2.

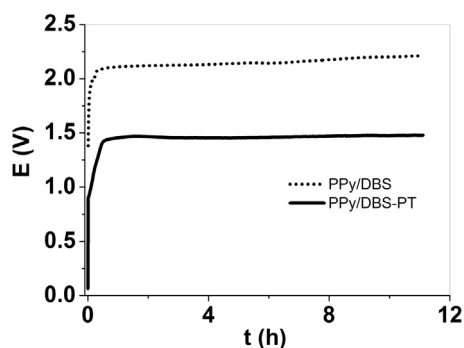


Fig. 1. Polymerisation curves of PPy/DBS (dotted) and PPy/DBS-PT (black). Polymerisation was performed in 1.8 mA and -20°C in solution consisting of ethylene glycol and water in ratio 1:1 in a 2-electrode cell of stainless steel sheet working electrode and stainless steel mesh counter electrode.

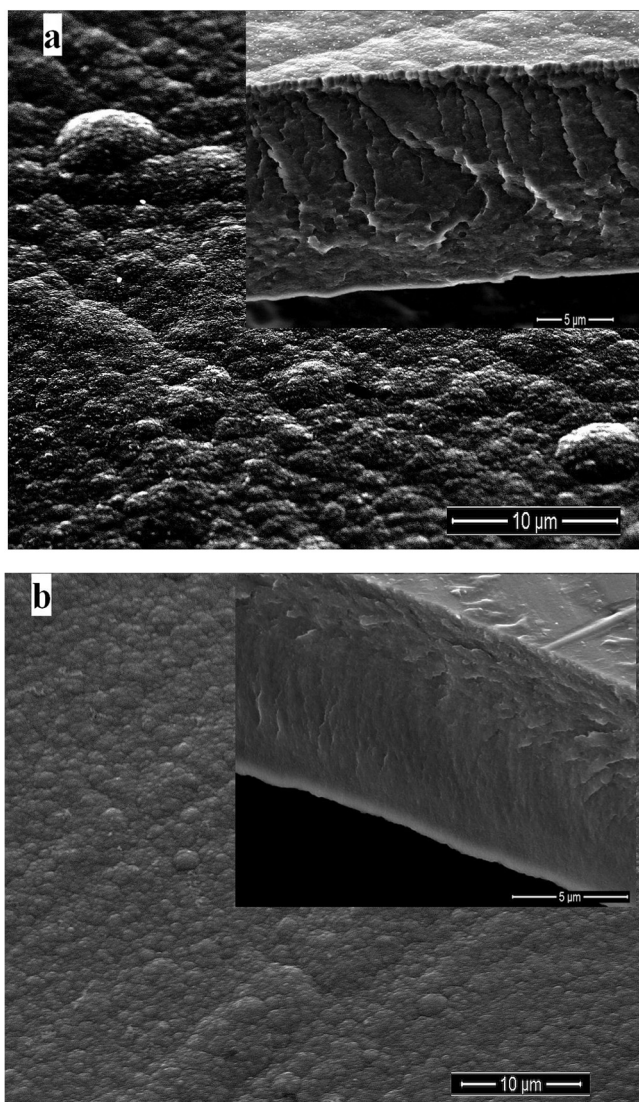


Fig. 2. SEM micrographs of surface (scale bar $10\ \mu\text{m}$) and cross section (inset, scale bar $5\ \mu\text{m}$) of films after polymerization in oxidized state (0.5 V) of a: PPy/DBS and b: PPy/DBS-PT.

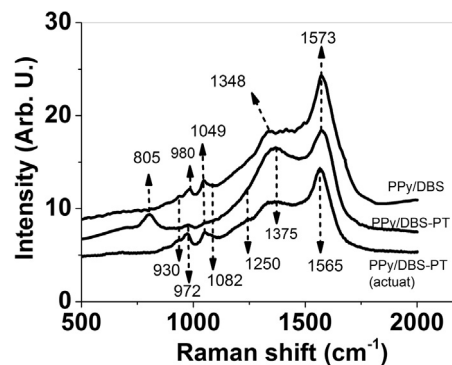


Fig. 3. Raman spectra ($1800\text{--}500\ \text{cm}^{-1}$, 514 nm) of: PPy/DBS, as-synthesized PPy/DBS-PT, and PPy/DBS-PT (after actuation of 600 redox cycles) in oxidized state (0.65 V).

3.2. SEM micrographs

PPy/DBS films showed a typical rough surface morphology with less compact structure (inset cross section, Fig. 2a). The surface of PPy/DBS-PT (Fig. 2b) is different from PPy/DBS showing a smoother morphology with more compact film formation (Fig. 2b, inset). The conductivity of the free-standing films before actuation (in oxidized state) of PPy/DBS and PPy/DBS-PT was found to be $0.5 \pm 0.04\ \text{S cm}^{-1}$ and $8.5 \pm 0.5\ \text{S cm}^{-1}$, respectively.

3.3. Spectroscopic characterisation of PPy/DBS and PPy/DBS-PT films

There are controversial opinions about the retention of POM during charging/discharging processes. Otero et al. [29] proposed that PPy/POM films cycled in LiClO_4 acetonitrile electrolyte partly lose POM, being replaced by ClO_4^- anions, which was detected over a mass loss of the films before and after charging/discharging reactions. Sung et al. [30] showed that in aqueous solutions of different electrolytes, no leaching of POM takes place. In order to verify if PT content is stable in our PPy/DBS-PT films during actuation, FTIR spectroscopy (Supplementary Fig. S1) and Raman measurements (Fig. 3) were performed.

The Raman spectra for PPy/DBS, as-prepared PPy/DBS-PT and PPy/DBS-PT after actuation are shown in Fig. 3, with the typical PPy Raman shifts at $1573\ \text{cm}^{-1}$ (C=C stretching [31]), $1348\ \text{cm}^{-1}$ (C–C stretching [31]) and $1250\ \text{cm}^{-1}$ (C–H in plane asymmetric bending [32]). The typical structure of the doped PPy film is shown by the peaks at $932\ \text{cm}^{-1}$ (ring deformation [31]) and $1082\ \text{cm}^{-1}$ (to C–H in-plane symmetric bending [31]), which are associated to the bipolaron structure and those at $980\ \text{cm}^{-1}$ (C–H bending [31] with evidence to cationic behaviour [32]) and $1049\ \text{cm}^{-1}$ (in plane symmetric bending [31]) are associated to the polaron structure [33]. PPy/DBS-PT (actuated) showing (Fig. 3) a small shift of the C=C stretching peak $1573\ \text{cm}^{-1}$ to $1565\ \text{cm}^{-1}$ which refers to PPy films with higher conductivities [34], which were in case of PPy/DBS-PT after actuation 17 times higher in comparison to PPy/DBS. The Raman spectra of the Keggin heteropolyacid has been investigated before with Raman shifts between 904 and $1007\ \text{cm}^{-1}$ [35], which cannot be observed here in PPy/DBS-PT spectra's (Fig. 3) due to the overlapping with PPy peaks between 930 and $1050\ \text{cm}^{-1}$. One sharp peak at $805\ \text{cm}^{-1}$ was observed for PPy/DBS-PT which shows the WO_3 (tungsten trioxide, crystalline form) attributed to the symmetric stretching vibration of the double bonded tungsten-terminal oxygen species [35]. In PPy/DBS-PT actuated, this peak is not detected anymore, which either means that residues of PT on the surface of PPy/DBS-PT film got removed from there after several redox cycles or that the form of PT has changed during actuation

cycles. FTIR measurements are presented in supplementary (Fig. S1). The main peaks for PPy/DBS (Fig. S1) were found at 1521 cm^{-1} assigned to N–H bending [36], 1436 cm^{-1} (C–C stretching vibration [37]), 1278 cm^{-1} (C–N stretching), 1030 cm^{-1} and $1130\text{--}1140\text{ cm}^{-1}$ are attributed to the bending vibration of pyrrole (polaron and bipolaron bands appear between 1045 and 1190 cm^{-1} [38]), and 885 cm^{-1} shows with little shift (871 cm^{-1} [37]) the C–H in plane vibrations. All PPy signals can be found in PPy/DBS-PT and PPy/DBS-PT (after actuation) spectra's (Fig. S1) with additional peaks at 1070 cm^{-1} (P–O stretching vibration [37]) and 963 cm^{-1} (W–O stretching vibrations [37]) revealing that PT anions are incorporated in PPy/DBS network.

3.4. Isometric stress and isotonic strain cyclic voltammetric measurements

Isometric stress and isotonic strain measurements were performed under cyclic voltammetric driving signals. The results of PPy/DBS free standing film and PPy/DBS-PT free standing film are presented in Fig. 4. It needs to be noted that the film thickness of PPy/DBS and PPy/DBS-PT was somewhat unequal, $19\text{ }\mu\text{m}$ and $23\text{ }\mu\text{m}$, respectively.

PPy/DBS films (Fig. 4a and b) showed strain in range of 1.9% and stress in range of 0.62 MPa at reduction; due to the immobilised anionic species (DBS^-), the solvated Li^+ cations are dragged into the film inducing volume change. The similarly prepared PPy/DBS-PT (Fig. 4a and b) linear actuators achieved stress in range of 0.86 MPa and strain of 3.8%. The CV curve in Fig. 4c shows for PPy/DBS a broad oxidation peak at 0.33 V and a reduction wave at -0.3 V . For PPy/DBS-PT films, the oxidation peak shifted to -0.03 V and the reduction wave to -0.25 V . The redox properties of PTA are strongly dependent on the nature of counter cations and solvents [39]. Counter cations influence the structure, where it was found that for the smaller type such as Li^+ or Na^+ the reduction wave is shifted towards more positive values [39]. The higher current density of PPy/DBS-PT in comparison to PPy/DBS is reflected in the higher charge density curves (Fig. 4d), PPy/DBS films showing charge density in range of 78 C cm^{-3} while PPy/DBS-PT having 1.4 times higher charge density of 111.3 C cm^{-3} . In earlier reports, the higher charging/discharging rates of PTA containing conducting polymers [18] has been also related to the higher amount of solvated counter-ions. In the present case, it was also observed that after immersing dry actuators in the working electrolyte solution, the PPy/DBS-PT films swelled up some 20% more than PPy/DBS films ($+10\text{ }\mu\text{m}$ vs $+8\text{ }\mu\text{m}$).

Keeping in mind that the concentration of PTA in the electropolymerisation solution is low (0.01 M) in comparison to NaDBS (0.1 M), we assume that the ratio of species incorporated into PPy during electropolymerisation is similar. Nevertheless, the effect on the properties of the material is substantial, as the PPy/DBS-PT showed 2 times higher strain with concurrent higher charge density. The relation is logical, as conducting polymers are faradaic actuators where based on the ESCR model, the exchanged charge density determines the actuation properties [12].

3.5. Chronoamperometric isometric stress and isotonic strain measurements

The PPy/DBS and PPy/DBS-PT linear actuators were submitted to consecutive square potential waves at different frequencies (0.1 Hz–0.0025 Hz) in LiTFSI aqueous electrolyte for measuring strain (Fig. 5a) and stress (Fig. 5b) response in potential range 0.65 V to -0.6 V , and coulodynamic Q-strain (Fig. 5c) and Q-stress (Fig. 5d) responses.

The chronodynamic (strain-time) actuator response (Fig. 5a) shows for PPy/DBS-PT strain in range of 5.2% and PPy/DBS strain at

2.1% with main expansion at reduction. PPy/DBS-PT films reached stress of 0.8 MPa which is 1.45 times higher than the stress observed for PPy/DBS linear actuators (0.55 MPa). In Fig. 5b, the stress of PPy/DBS-PT films decreased at applied potential of 0.65 V, which can be explained by relaxation and creep effects of conducting polymers, seen before elsewhere [40]. The effect so far cannot be observed in the strain curve (Fig. 5a).

The current density curves against time are shown in Fig. S2 (Supplementary) with much higher current density observed for PPy/DBS-PT than PPy/DBS. The integration of the current density time curve for each step gives the charge density shown in Fig. S3a for the oxidation and reduction (Fig. S3b) for each applied frequency. The low frequency of 0.0025 Hz (Fig. S3a and b) exhibit highest charge density that as an example at oxidation of PPy/DBS was found in range of 70.43 C cm^{-3} and for PPy/DBS-PTA at 131.2 C cm^{-3} , as expected for a material of interest for energy storage applications. For both films, the charge decreased with increasing frequency (Fig. S3a and b). High charge density (low frequency) corresponds to high strain and stress while low charge density (high frequency) leads to low strain and stress. The coulodynamic strain-Q (Fig. 5c) and stress-Q (Fig. 5d) describe faradaic actuators at applied frequencies 0.1 Hz–0.0025 Hz, where the strain and stress follow a linear dependency of the consumed charge [6]. Long-term measurements (200 cycles between 0.65 V to -0.6 V at 0.1 Hz) of strain were performed (Fig. S4a–d). For PPy/DBS films, 0.6% strain was found (Fig. S4a and b) at charge density of 4.25 C cm^{-3} , and for PPy/DBS-PTA the strain was 2% with charge density of 4.6 C cm^{-3} . For both samples the strain remained virtually constant during the 200 cycles (Fig. S4a–d).

3.6. Chronopotentiometric isometric stress and isotonic strain measurements

The linear actuators were further characterized by square current waves, under different frequencies, each wave involving the same charge of 1 mC. To obtain the specific capacitance C_s of the material, the slope after the IR drop during reduction was calculated by applying Eq. (1) with current I and volume of the film (area*thickness).

$$C_s = \frac{I}{-\text{slope} * \text{Volume}} \quad (1)$$

The potential response to two square current waves for PPy/DBS and PPy/DBS-PT at applied frequency 0.005 Hz and the specific capacitance C_s as a function of frequency are presented in Fig. 6.

The specific capacitance C_s of PPy/DBS-PT and PPy/DBS linear actuators (Fig. 6b) was calculated following Eq. (3), indicating nearly 1.8 times higher maximum specific capacitance (143 F/g) for PPy/DBS-PT in comparison to PPy/DBS (80 F/g). Therefore, even a small addition of PTA in the electropolymerisation solution increases the specific capacitance of PPy significantly.

3.7. EDX spectra of PPy/DBS-PTA

The EDX spectra, featuring peaks of carbon (C), oxygen (O), sodium (Na), Tungsten (W), phosphorus (P) and sulphur (S) are presented in Fig. 7.

The Na peak at 1.04 keV for PPy/DBS (Supplementary, Fig. S5) and PPy/DBS-PT (Fig. 7) films are residues from the electropolymerization. The sulphur peak at 2.32 keV, the oxygen peak at 0.52 keV and the carbon peak at 0.26 keV remain virtually unchanged after oxidation and reduction (Figs. S5 and 7). The immobilized DBS^- ions in PPy/DBS and PPy/DBS-PT films are reflected in the sulphur and oxygen peaks, which shows no significant change during the redox cycles in aqueous electrolyte. As for PTA, the typical tungsten peak at 1.78 keV is followed by a small broad peak for phosphorus

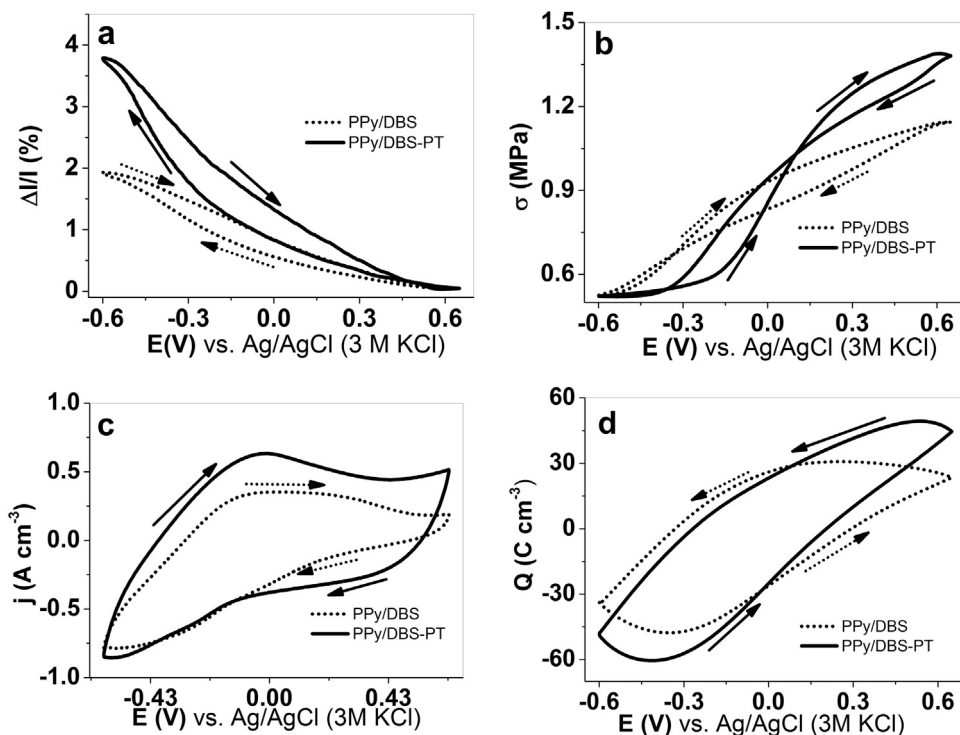


Fig. 4. Isometric stress and isotonic strain cyclic voltammetric measurements (scan rate 5 mV/s, 5th cycle) of PPy/DBS (dotted) and PPy/DBS-PT (solid) in LiTFSI-aq electrolyte in potential range 0.65 V to -0.6 V in a three electrode setup (working electrode: free-standing film, counter electrode: platinum sheet, reference electrode: Ag/AgCl (3 M KCl)) of a: strain $\Delta l/l$ (%) vs. potential E (applied stress: PPy/DBS 0.52 MPa and for PPy/DBS-PT 0.43 MPa); b: stress σ (MPa) vs. potential E; c: current density j vs. E; and d: charge density Q vs. E.

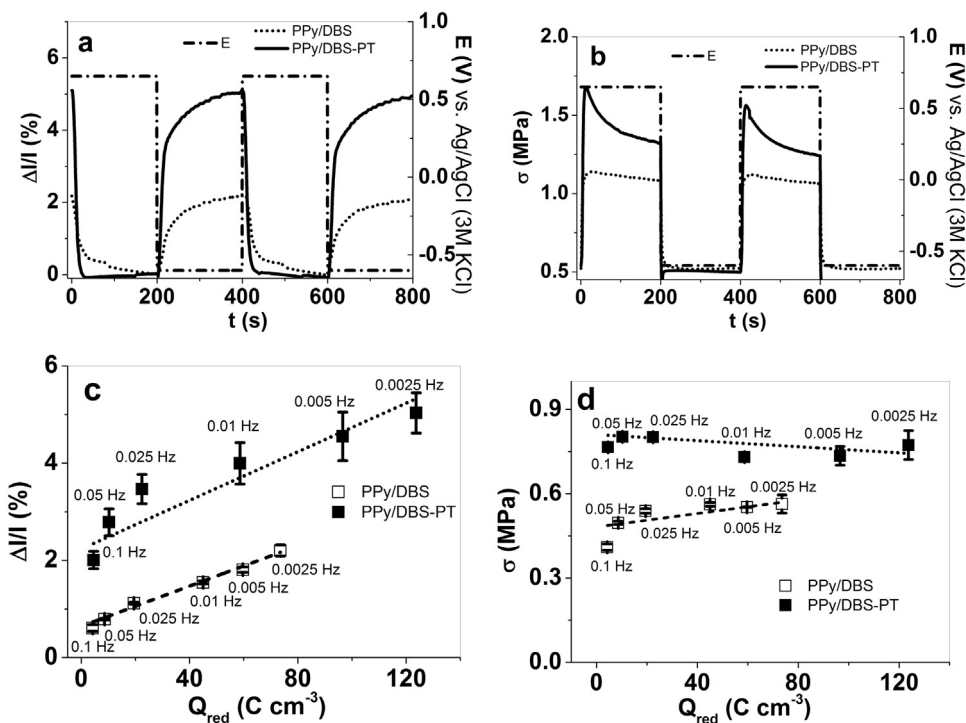


Fig. 5. Isometric stress and isotonic strain square wave potential measurements of PPy/DBS (dotted) and PPy/DBS-PT (solid line) in LiTFSI-aq electrolyte at potential range 0.65 V to -0.6 V in a three electrode system (counter electrode: platinum sheet, reference electrode: Ag/AgCl (3 M KCl)) of a: 2 cycles of strain response to potential steps at 0.0025 Hz, b: 2 cycles of stress response to potential steps at 0.0025 Hz frequency. c: strain values (average values with linear fit) at frequencies 0.0025 Hz–0.1 Hz (applied stress: PPy/DBS 0.52 MPa and; PPy/DBS-PT 0.43 MPa), and d: stress values σ (MPa) against charge density Q_{red} (normalised). In c) and d), the frequencies corresponding to the charge densities are shown as labels.

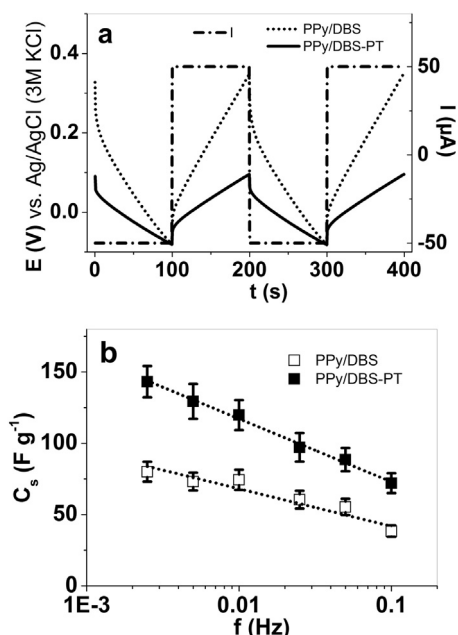


Fig. 6. Chronopotentiometric isometric stress and isotonic strain (constant charge of 1 mC) measurements of PPy/DBS (dotted, □) and PPy/DBS-PT (solid, ■) in LiTFSI-aq electrolyte in a three-electrode system (counter electrode platinum sheet, reference electrode: Ag/AgCl (3 M KCl)) of a: potential vs time at 0.005 Hz frequency with current $\pm 50 \mu\text{A}$ (dash-dot-dash), b: specific capacitance C_s against applied frequency f .

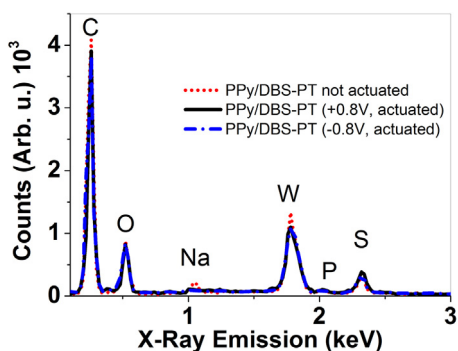


Fig. 7. EDX spectra (0.1–3 keV) of PPy/DBS-PT linear films not actuated (red, dotted), actuated and oxidized (solid black) at 0.8 V (5 min), and actuated and reduced (blue, dash dot dash) at -0.8V (5 min). (For interpretation of the references to colour in this figure legend, the reader is referred to the web version of this article.)

at 2.02 keV. While conclusive quantitative comparisons are difficult to make from such spectra, the tungsten peak is still clearly observed after actuation (Fig. 7). There is also no indication of it being replaced by TFSI⁻, as no fluorine signal is detected after actuation.

From FTIR (Supplementary section, Fig. S1), Raman and EDX spectra, it can be summarized that a) PTA is definitely incorporated into PPy films during electropolymerisation, and b) at least most part of it is retained in the film during redox cycling/actuation in aqueous electrolyte and does not get replaced by TFSI⁻ ions.

4. Conclusion

Freestanding PPy/DBS and PPy/DBS-PT films were compared using a variety of methods, with the focus on their linear actuation properties. The small addition of PTA during electropolymerisation remarkably changes virtually every aspect, starting from the significantly lowered synthesis potential, due to the electrocat-

alytic effect. As a result, more compact, expandable films are formed, with higher conductivity and improved electrochemical and electro-chemo-mechanical characteristics. The cation-driven actuators showed 3.4 times higher strain and 5 times higher stress than the PPy/DBS analogues. The improved actuation response of PPy/DBS-PT is mainly attributed to the higher conductivity, in turn leading to higher exchanged charge (in same time-scale), here manifested as higher specific capacitance. The FTIR, Raman, and EDX spectra confirmed that tungsten gets incorporated during the synthesis and at least in most part stays in the film during the redox cycling/actuation. The higher electro-chemo-mechanical response is even more significant if one considers the somewhat higher thickness and weight/density of the PPy/DBS-PT samples.

Acknowledgements

The research was supported by European Union's Horizon 2020 research and innovation program under the Marie Skłodowska-Curie grant agreement No. 641822 and partly by the European Union through the European Social Fund (MTT76) and Estonian Research Council Grant IUT20-24.

Appendix A. Supplementary data

Supplementary data associated with this article can be found, in the online version, at <http://dx.doi.org/10.1016/j.snb.2017.03.061>.

References

- [1] S. Hara, T. Zama, S. Sewa, W. Takashima, K. Kaneto, Highly stretchable and powerful polypyrrole linear actuators, *Chem. Lett.* 32 (2003) 576–577, <http://dx.doi.org/10.1246/cl.2003.576>.
- [2] R. Kiefer, P.A. Kilmartin, G.A. Bowmaker, R.P. Cooney, J. Travas-Sejdic, Actuation of polypyrrole films in propylene carbonate electrolytes, *Sens. Actuators B Chem.* 125 (2007) 628–634, <http://dx.doi.org/10.1016/j.snb.2007.03.008>.
- [3] A. Maziz, A. Khaldi, N.-K. Persson, E.W.H. Jager, Soft linear electroactive polymer actuators based on polypyrrole, *Proc. SPIE* 9430 (2015) 943016, <http://dx.doi.org/10.1117/12.2081821>.
- [4] S. Hara, T. Zama, W. Takashima, K. Kaneto, TFSI-doped polypyrrole actuator with 26% strain, *J. Mater. Chem.* 14 (2004) 1516, <http://dx.doi.org/10.1039/b404232h>.
- [5] R. Kiefer, G.A. Bowmaker, P.A. Kilmartin, J. Travas-Sejdic, Effect of polymerization potential on the actuation of free standing poly-3 4-ethylenedioxythiophene films in a propylene carbonate electrolyte, *Electrochim. Acta* 55 (2010) 681–688, <http://dx.doi.org/10.1016/j.electacta.2009.09.034>.
- [6] J.G. Martinez, T.F. Otero, E.W.H. Jager, Effect of the electrolyte concentration and substrate on conducting polymer actuators, *Langmuir* 30 (2014) 3894–3904, <http://dx.doi.org/10.1021/la404353z>.
- [7] R. Kiefer, J.G. Martinez, T.F. Otero, A. Kesküla, F. Kaasik, M. Harjo, R. Valner, V. Vaddeppally, A.-L. Peikola, A. Aabloo, Solvent and electrolyte effects in PPY/DBS free standing films, *SPIE Smart Struct. Mater. Nondestruct. Eval. Health Monit.* 9430 (2015) 94301C, <http://dx.doi.org/10.1117/12.2084195>.
- [8] T.F. Otero, M. Alfaro, Oxidation kinetics of polypyrrole films: solvent influence, *JEAC* (2016), <http://dx.doi.org/10.1016/j.jelechem.2016.07.043>, accepted.
- [9] S. Hara, T. Zama, Free-standing gel-like polypyrrole actuators doped with bis(perfluoroalkylsulfonate) imide exhibiting extremely large strain, *Smart Mater. Struct.* 14 (2005) 1501–1510, <http://dx.doi.org/10.1088/0964-1726/14/6/042>.
- [10] E. Smela, Conjugated polymer actuators for biomedical applications, *Adv. Mater.* 15 (2003) 481–494.
- [11] R. Kiefer, N. Aydemir, J. Torop, T. Tamm, R. Temmer, J. Travas-Sejdic, I. Must, F. Kaasik, A. Aabloo, Carbide-derived carbon as active interlayer of polypyrrole tri-layer linear actuator, *Sens. Actuators B Chem.* 201 (2014) 100–106, <http://dx.doi.org/10.1016/j.snb.2014.04.093>.
- [12] R. Kiefer, J.G. Martinez, A. Kesküla, G. Anbarjafari, A. Aabloo, T.F. Otero, Polymeric actuators: Solvents tune reaction-driven cation to reaction-driven anion actuation, *Sens. Actuators B Chem.* 233 (2016) 328–336, <http://dx.doi.org/10.1016/j.snb.2016.04.090>.
- [13] N. Aydemir, P.A. Kilmartin, J. Travas-Sejdic, A. Kesküla, A.-L. Peikola, J. Parcell, M. Harjo, A. Aabloo, R. Kiefer, Electrolyte and solvent effects in PPY/DBS linear actuators, *Sens. Actuators B Chem.* 216 (2015) 24–32, <http://dx.doi.org/10.1016/j.snb.2015.03.098>.
- [14] S. Cheng, T. Fernández-Otero, E. Coronado, C.J. Gómez-García, E. Martínez-Ferrero, C. Giménez-Saiz, Hybrid material polypyrrole/[SiCr(H₂O)W₁₁O₃₉]⁵⁻: electrogeneration, properties, and stability

- under cycling, *J. Phys. Chem. B* 106 (2002) 7585–7591, <http://dx.doi.org/10.1021/jp014340y>.
- [15] S. Herrmann, C. Ritchie, C. Streb, Polyoxometalate–conductive polymer composites for energy conversion, energy storage and nanostructured sensors, *Dalton Trans.* 44 (2015) 7092–7104, <http://dx.doi.org/10.1039/C4DT03763D>.
- [16] B.B. Xu, M. Lu, J.H. Kang, D. Wang, J. Brown, Z.H. Peng, Synthesis and optical properties of conjugated polymers containing polyoxometalate clusters as side-chain pendants, *Chem. Mater.* 17 (2005) 2841–2851, <http://dx.doi.org/10.1021/cm050188r>.
- [17] M. Genovese, K. Lian, Polyoxometalate modified inorganic-organic nanocomposite materials for energy storage applications: a review, *Curr. Opin. Solid State Mater. Sci.* 19 (2015) 126–137, <http://dx.doi.org/10.1016/j.cossms.2014.12.002>.
- [18] T.F. Otero, S.A. Cheng, E. Coronado, E.M. Ferrero, C.J. Gomez-Garcia, Functional hybrid materials containing polypyrrole and polyoxometalate clusters: searching for high conductivities and specific charges, *Chemphyschem* 3 (10) (2002) 808, [http://dx.doi.org/10.1002/1439-7641\(20020916\)3:9<808::AID-CPHC808>3.0.CO;2-U](http://dx.doi.org/10.1002/1439-7641(20020916)3:9<808::AID-CPHC808>3.0.CO;2-U).
- [19] G.M. Suppes, B.A. Deore, M.S. Freund, Porous conducting polymer/heteropolyoxometalate hybrid material for electrochemical supercapacitor applications, *Langmuir* 24 (2008) 1064–1069, <http://dx.doi.org/10.1021/la702837j>.
- [20] G.M. Suppes, C.G. Cameron, M.S. Freund, A polypyrrole/phosphomolybdic acidpoly(3,4-ethylenedioxythiophene)/phosphotungstic acid asymmetric supercapacitor, *J. Electrochem. Soc.* 157 (2010) A1030, <http://dx.doi.org/10.1149/1.3464802>.
- [21] A.M. White, R.C.T. Slade, Polymer electrodes doped with heteropolymetallates and their use within solid-state supercapacitors, *Synth. Met.* 139 (2003) 123–131, [http://dx.doi.org/10.1016/S0379-6779\(03\)00039-0](http://dx.doi.org/10.1016/S0379-6779(03)00039-0).
- [22] A.K. Cuentas-Gallegos, R. Martínez-Rosales, M. Baibarac, P. Gómez-Romero, M.E. Rincón, Electrochemical supercapacitors based on novel hybrid materials made of carbon nanotubes and polyoxometalates, *Electrochem. Commun.* 9 (2007) 2088–2092, <http://dx.doi.org/10.1016/j.elecom.2007.06.003>.
- [23] J. Hou, G. Zhu, J. Zheng, Synthesis, characterization and corrosion protection study of polypyrrole/phosphotungstate coating on low alloy steel in seawater, *Polym. Sci. Ser. B* 53 (2011) 546–552, <http://dx.doi.org/10.1134/S1560090411100034>.
- [24] M. Zhou, L. Guo, F. Lin, H. Liu, Electrochemistry and electrocatalysis of polyoxometalate-ordered mesoporous carbon modified electrode, *Anal. Chim. Acta* 587 (2007) 124–131, <http://dx.doi.org/10.1016/j.aca.2007.01.017>.
- [25] Z. Kang, Y. Wang, E. Wang, S. Lian, L. Gao, W. You, C. Hu, L. Xu, Polyoxometalates nanoparticles: synthesis, characterization and carbon nanotube modification, *Solid State Commun.* 129 (2004) 559–564, <http://dx.doi.org/10.1016/j.ssc.2003.12.012>.
- [26] J. Vaillant, M. Lira-Cantu, K. Cuentas-Gallegos, N. Casan-Pastor, P. Gomez-Romero, Chemical synthesis of hybrid materials based on PANi and PEDOT with polyoxometalates for electrochemical supercapacitors, *Prog. Solid State Chem.* 34 (2006) 147–159, <http://dx.doi.org/10.1016/j.progsolidstchem.2005.11.015>.
- [27] Z. Zondaka, R. Valner, T. Tamm, A. Aabloo, R. Kiefer, Carbide-derived carbon in polypyrrole changing the elastic modulus with a huge impact on actuation, *RSC Adv.* 6 (2016) 26380–26385, <http://dx.doi.org/10.1039/c6ra01511e>.
- [28] M. Plaado, F. Kaasik, R. Valner, E. Lust, R. Saar, K. Saal, A. Peikolainen, A. Aabloo, R. Kiefer, Electrochemical actuation of multiwall carbon nanotube fiber with embedded carbide-derived carbon particles, *Carbon (N.Y.)* 94 (2015) 911–918, <http://dx.doi.org/10.1016/j.carbon.2015.07.077>.
- [29] T.F. Otero, S.A. Cheng, F. Huerta, Hybrid materials polypyrrole/PW₁₂O₄₀³⁻. 1. Electrochemical synthesis, kinetics and specific charges, *J. Phys. Chem. B* 104 (2000) 10522–10527, <http://dx.doi.org/10.1021/jp000553w>.
- [30] H. Sung, H. So, W.K. Paik, Polypyrrole doped with heteropolytungstate anions, *Electrochim. Acta* 39 (1994) 645–650, [http://dx.doi.org/10.1016/0013-4686\(94\)80005-7](http://dx.doi.org/10.1016/0013-4686(94)80005-7).
- [31] X. Zou, Y. Shen, Z. Peng, L. Zhang, L. Bi, Y. Wang, S. Dong, Preparation of a phosphopolyoxomolybdate P2Mo18O626- doped polypyrrole modified electrode and its catalytic properties, *J. Electroanal. Chem.* 566 (2004) 63–71, <http://dx.doi.org/10.1016/j.jelechem.2003.11.012>.
- [32] K. Crowley, J. Cassidy, In situ resonance Raman spectroelectrochemistry of polypyrrole doped with dodecylbenzenesulfonate, *J. Electroanal. Chem.* 547 (2003) 75–82, [http://dx.doi.org/10.1016/S0022-0728\(03\)00191-8](http://dx.doi.org/10.1016/S0022-0728(03)00191-8).
- [33] S. Demoustier-Champagne, P.-Y. Stavaux, Effect of electrolyte concentration and nature on the morphology and the electrical properties of electropolymerized polypyrrole nanotubules, *Chem. Mater.* 11 (1999) 829–834, <http://dx.doi.org/10.1021/cm9807541>.
- [34] Y.-C. Liu, B.-J. Hwang, Identification of oxidised polypyrrole on Raman spectrum, *Synth. Met.* 113 (2000) 203–207, [http://dx.doi.org/10.1016/S0379-6779\(00\)00188-0](http://dx.doi.org/10.1016/S0379-6779(00)00188-0).
- [35] S.R. Matkovic, L.E. Briand, M.A. Banares, Investigation of the thermal stability of phosphotungstic Wells-Dawson heteropoly-acid through in situ Raman spectroscopy, *Mater. Res. Bull.* 46 (2011) 1946–1948, <http://dx.doi.org/10.1016/j.materresbull.2011.07.015>.
- [36] V.K. Gade, D.J. Shirale, P.D. Gaikwad, K.P. Kakde, P.A. Savale, H.J. Kharat, M.D. Shirsat, Synthesis and characterization of Ppy-PVS, Ppy-pTS, and Ppy-DBS composite films, *Int. J. Polym. Mater.* 56 (2007) 107–114, <http://dx.doi.org/10.1080/00914030600735155>.
- [37] J. Bonastre, J. Molina, J.C. Galvan, F. Cases, Characterization of polypyrrole/phosphotungstate membranes by electrochemical impedance spectroscopy, *Synth. Met.* 187 (2014) 37–45, <http://dx.doi.org/10.1016/j.synthmet.2013.10.020>.
- [38] H.K. Lim, S.O. Lee, K.J. Song, S.G. Kim, K.H. Kim, Synthesis and properties of soluble polypyrrole doped with dodecylbenzenesulfonate and combined with polymeric additive poly(ethylene glycol), *J. Appl. Polym. Sci.* 97 (2005) 1170–1175, <http://dx.doi.org/10.1002/app.21824>.
- [39] S. Himeno, M. Takamoto, Difference in voltammetric properties between the Keggin-type [XW₁₂O₄₀]ⁿ⁻ and [XMo₁₂O₄₀]ⁿ⁻ complexes, *J. Electroanal. Chem.* 528 (2002) 170–174.
- [40] K. Kaneto, Research trends of soft actuators based on electroactive polymers and conducting polymers, *J. Phys. Conf. Ser.* 704 (2016) 12004, <http://dx.doi.org/10.1088/1742-6596/704/1/012004>.

Biographies

Zane Zondaka currently is a PhD student at University of Tartu with main focus of composite materials; consisting of embedded carbon based particles in conducting polymers. She received her M.Sc degree in Riga Technical University in Nano engineering at the year 2014.

Arko Kesküla is a PhD student at University of Tartu (IMS lab) with main focus on polymeric ionic liquids as membranes for electrochemical actuators under supervision of Dr. A.-L. Peikolainen and Prof. Uno Mäeorg. He received his master degree 2012 at University of Tartu in material science.

Tarmo Tamm, born in Tartu, Estonia, received both his MSc and PhD degrees in chemistry at the University of Tartu. At present, he is a senior research fellow of material sciences at University of Tartu, Estonia. His research interests are mainly related to both the experimental and theoretical characterization of materials, especially conducting polymers.

Rudolf Kiefer received his diploma in chemistry (MSc) from University of Freiburg, (Germany) in 1999 and his PhD degree (conducting polymers for micro actuators) in micro system techniques from Freiburg University (Germany) in 2005. He made his post doc at the Polymer Electronic Research Centre (PERC) of University of Auckland, New Zealand and worked in Industrial Technology Research Institute in Hsinchu, Taiwan as a researcher and in University of Tartu (Estonia) as a visiting professor and senior researcher. Since 2016 he is Associate Professor at Ton Duc Thang University, Vietnam. His main research interest includes characterization and applications in electro active polymers.